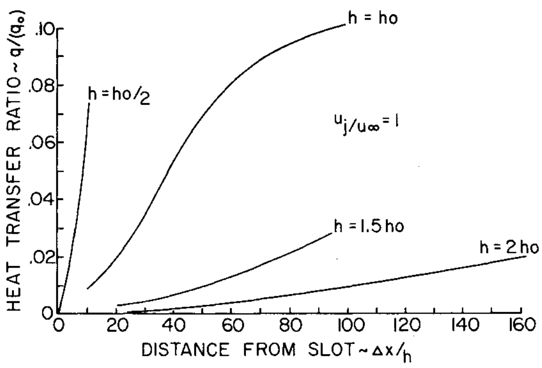

Fig. 2 Heat-transfer ratio vs distance from slot for various slot heights.

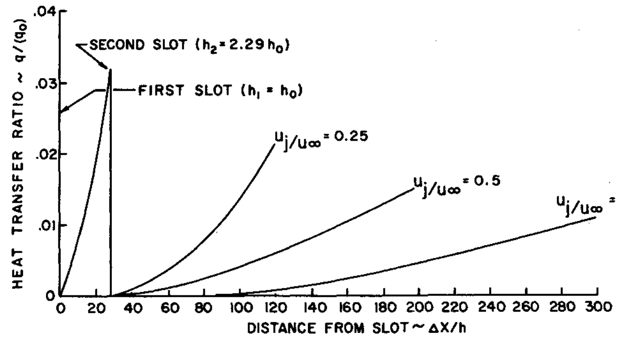

Fig. 3 Heat-transfer ratio vs distance from slot for double slot configuration.

select ξ_0 to obtain a dimensional slot height h_0 that was physically significant.

To examine the effect of slot height, jet velocity, and the second slot, a number of cases have been examined. These are shown in Table 1.

Figure 1 shows the effect of jet velocity on heat transfer to the surface. The peak in Fig. 1 for $u_j/u_\infty = 0.5$ is due to the $\xi^{-0.5}$ variation of the heat transfer [i.e., Eq. (4)]. The effect of slot height is shown in Fig. 2. Here, it can be seen that slot height is much more important in reducing heat transfer than jet velocity. In Fig. 2, the distance to $q/q_0 = 0.02$ for $h = 2h_0$ is $162h_0$. For the same coolant flow in Fig. 1, $q/q_0 = 0.02$ is reached at a distance of $44h_0$ for $u_j/u_\infty = 2.0$.

Figure 3 presents the results for a double slot configuration. The location of the second slot is dictated by design limitations on the heat transfer to the wall. For an 8000°K main flow temperature, the black body radiation which is not affected by film cooling is 2.25 kw/cm^2 and the zero injection convection at the slot is approximately 18 kw/cm^2. Assuming a maximum allowable heating of 3 kw/cm^2, it is reasonable to limit the convection with film cooling to 25% of the radiation heating.

This condition requires that the second slot be introduced 20 slot heights, downstream of the first slot. The jet velocity ratio at the second slot was varied from 0.25 to 1.0. The second slot was the same height as the first in η coordinates or $2.29h_0$ in physical dimensions. From Fig. 3, it can be seen that the second slot is more effective than the first. For a $u_j/u_\infty = 1.0$ at the second slot, the distance protected is increased by a factor of ten ($300h_0$ vs $30h_0$).

In film cooling, the most significant parameter is the coolant mass flow required. For the cases considered in this study, the coolant mass flow is proportional to

$$[(u_j/u_\infty)_1 h_1 + (u_j/u_\infty)_2 h_2]$$

Table 2 shows comparison of the protection ($q/q_0 < 0.032$) provided by three different film cooling configurations.

This study has provided results for film cooling by means of tangential injection into a laminar boundary layer. The calculations have shown that for the same coolant mass flow increasing slot thickness is a more effective means of reducing heat transfer than increasing jet velocity. The introduction of a second slot can provide a significant increase in protection when compared to the single slot cases.

The next phase of this study is the examination of the turbulent case. Turbulent mixing tends to be more rapid than laminar mixing, thereby reducing the cooling effectiveness with distance. However, the turbulent heat-transfer rates with or without injection decrease as $\xi^{-0.8}$ compared to $\xi^{-0.5}$ for laminar flow; hence the two effects tend to counteract each other so that qualitatively the results obtained herein might be indicative of what happens for turbulent flow.

Table 2 Comparison of protection methods

Configuration	Distance protected	Coolant mass flow parameter
Single slot		
$(h = h_0, u_j/u_\infty = 2.0)$	$58h_0$	2
$(h - 1.5h_0, u_j/u_\infty = 1.0)$	$100h_0$	1.5
Double slot		
$h_1 = h_0, u_j/u_\infty = 1.0$	$140h_0$	1.57
$h_2 = 2.29h_0, u_j/u_\infty = 0.5$		

References

[1] Blottner, F. G., "Non-Equilibrium Laminar Boundary Layer Flow of a Binary Gas," GE TIS R63SD17, June 1963, General Electric Co., Philadelphia, Pa.

[2] Sherman, A., Yeh, H., McAssey, E., Jr., and Reshotko, E., "Summary Report MHD Boundary Layers with Non-Equilibrium Ionization and Finite Rates," June 1970, Computer and Applied Sciences Inc., Norristown, Pa.

Application of Nonlinear Estimators to Hereditary Systems

J. R. SCHIESS* AND V. R. ROLAND*
NASA Langley Research Center, Hampton, Va.

AND

W. R. WELLS†
University of Cincinnati, Cincinnati, Ohio

BECAUSE of the increasing importance of dynamic processes with time delays, the study of the optimal control and estimation of hereditary systems has been intensified during the past decade. Various authors have shown the effect of the dead time to be important in such diverse problems as the modeling

Presented as Paper 72-902 at the AIAA/AAS Astrodynamics Conference, Palo Alto, Calif., September 11–12, 1972; submitted October 5, 1972; revision received April 2, 1973.

Index category: Navigation, Control, and Guidance Theory.

* Aerospace Technologist.

† Associate Professor of Aerospace Engineering. Associate Fellow AIAA.

of human performance, chemical and industrial processes, and so forth.[1-2] Early work in the area of the state prediction of linear and nonlinear time delay systems has also been reported.[2-4] The work of Kwakernaak[4] on the linear problem concerned an estimate of the state but no parameters. Although an exact solution for the optimal filter is obtained, it presents practical computational difficulties. The results of Koivo[3] present an estimator (but not necessarily optimal) for both state and particular parameters excluding the time delay. More recently, Mehra[5] has utilized the maximum likelihood method to estimate the human operator time delay. The present paper presents the extended Kalman filter applied to delayed systems to determine both the state and the time delay. In addition, two nonlinear estimators as discussed in Ref. 6 are investigated. Since the intent of the analysis is to study the feasibility of extracting the time delay, it was felt the elementary problem of Koivo[3] and the two nonlinear filters were appropriate.

The vector form of a general system of nonlinear retarded differential-difference equations with process noise can be written as

$$\dot{x}(t) = f[x(t), x(t-\theta), a, t] + w(t) \tag{1}$$

where $x(t)$ is the n-dimensional state vector, a is the k-dimensional parameter vector, and θ is the constant time delay. The vector $w(t)$ is an n-dimensional vector representing the white noise process in the system. The general form of the noisy measurement vector is assumed to be

$$y(t) = h[x(t)] + v(t) \tag{2}$$

where y is m-dimensional and v is an m-dimensional white noise vector. The process and measurement noise are assumed to have zero means and diagonal covariance matrices. For the purpose of obtaining an estimate of the parameter vector, a, the state vector is extended to $n+k$-dimension of the state and parameter components.

In order to compare with the nonlinear results to follow, an extension of the Kalman-Bucy filter is considered at this point. The nonlinear system is linearized about a nominal trajectory $x^*(t)$. The result is a linear time varying system for $\alpha(t) \equiv x(t) - x^*(t)$ which when discretized has the form

$$\alpha(k+1) = \Phi(k+1, k)\alpha(k) + \Omega(k)\alpha(k-q) + w(k) \tag{3}$$

where to first order

$$\Phi(k+1, k) = I + \Delta t A(k), \quad \Omega(k) = \Delta t B(k) \tag{4}$$

The matrices $A(k)$ and $B(k)$ are the partials of f with respect to the current and delayed state, respectively; q is the ratio of the time delay to the time increment. If the assumption is made that the term $\Omega(k)\alpha(k-q)$ can be approximated at time t_k by using the value of α at t_{k-q}, then this term can be treated as a known forcing function in the filter equations resulting in the estimate

$$\hat{\alpha}(k+1/k) = \phi(k+1, k)\hat{\alpha}(k/k) + \Omega(k)\hat{\alpha}(k-q/k-q) \tag{5a}$$

$$\hat{\alpha}(k+1/k+1) = \hat{\alpha}(k+1/k) + F(k+1)[\beta(k+1) - H(k+1)\hat{\alpha}(k+1/k)] \tag{5b}$$

where $F(k+1)$ is the Kalman gain which can be computed from the matrix Riccati equation. The derivation is completed by linearizing the measurement equation.

The problem chosen for investigation is similar to the one given by Koivo.[3] The noise-free scalar equation of motion is

$$\ddot{x}(t) = -ax(t) - b\dot{x}(t-\theta) + u(t) \tag{6}$$

where $u(t)$ is a known forcing function. By transforming to the frequency domain, using Padé approximations of the exponential and retransforming to the time domain, the time delay can be made an explicit parameter. In the sequel, the parameters a, b, and θ are to be treated as state variables.

The known forcing function $u(t)$ was chosen to be $0.75 \cos \pi t/4$. For the initial conditions used to generate the measurements, all the variables and parameters were equal to 1.0 except the time delay which was 0.5. In all the cases considered, process noise with variance 0.0016 was added to Eq. (6). The differential-difference equation was numerically integrated to a final time of 20 sec with the measurements and the forcing function sampled every 0.01 sec. Both linear and nonlinear measurements were considered. For both data types the variance of the measurement noise was 0.0004.

The study considered three different models of the original equation. The first model, called the "pure" form, is the original Eq. (6) in which the delay occurs implicitly as the argument of a state variable. The other two models considered are those in which the time delay is made explicit by using first- and second-order Padé approximations. However, the advantage of having an explicit time delay must be weighed against the disadvantages of additional variables and possibly higher correlations.

In addition to the Kalman filter form described by Eq. (5) for the pure model, the standard Kalman filter was applied to the two Padé models. The nonlinear estimators chosen for study were the truncated minimal variance (TMV) and the dynamic programing least-squares (DPLS) filters which can be found in Schwartz and Stear.[6] The TMV filter was chosen because it represents the more complex nonlinear filters which require evaluation of the second partial derivatives of the state equations and measurement function. In contrast to this, the DPLS filter is a simpler nonlinear filter utilizing only the first-order partials. Although the TMV filter is more sophisticated than the DPLS filter, Schwartz and Stear[6] have shown that the nonlinear filters they studied provide approximately equal results which are better than the Kalman filter results. Therefore, this study considered the Kalman filter as the standard estimator and the two nonlinear filters as optional approaches.

In the results that follow, the root-mean-squared (rms) errors of the estimated variables and parameters at 20 sec are used as a basis for comparison. The rms errors are based on only a few cases for each study because of computer time limitations. Statistically, the results are not conclusive; however, based on the present data which are consistent for all the cases, the stated conclusions appear to be indicated.

The initial guesses of the variables and parameters were perturbed 10% from the true values; the initial variances were chosen so that these errors occurred at one standard deviation. The results obtained using only linear measurements are given in Table 1. The Kalman filter with the pure form diverges. However, an iterated version of this filter solved the divergence problem as indicated in Table 1. The estimates based on the Padé approximations are also improved with the estimates from the second-order approximation almost as good as the nonlinear filter estimates. In this study, a straightforward application of the original Kalman filter was emphasized; in a real application multiple passes through the data, possibly using modifications of the filter such as a limited memory filter, would be attempted. The truncated minimal variance filter performs well for all three

Table 1 Results obtained by using linear measurements with Kalman, truncated minimal variance (TMV), and dynamic programing least-squares (DPLS) filters

Model	Filter	Root-mean-squared errors at final time				
		x	$\dot{x}$	a	b	θ
Pure	Kalman	0.01926	0.07016	0.50589	0.25252	0.20317
Pure	Iterated Kalman	0.02149	0.03247	0.05794	0.09361	0.04173
First-order Padé	Kalman	0.01888	0.21246	0.07584	0.34084	0.05129
Second-order Padé	Kalman	0.01702	0.24877	0.09145	0.41419	0.02645
Pure	TMV	0.01788	0.00999	0.00913	0.04276	0.02142
First-order Padé	TMV	0.00897	0.00362	0.00566	0.00459	0.02315
Second-order Padé	TMV	0.01040	0.00707	0.01565	0.01204	0.01384
Pure	DPLS	0.01638	0.01234	0.00438	0.03875	0.02114
First-order Padé	DPLS	0.00493	0.00521	0.00706	0.00530	0.01920
Second-order Padé	DPLS	0.00545	0.00677	0.00927	0.00786	0.01400

models as Table 1 shows. The final entries in Table 1 show the results obtained using the dynamic programing least-squares filter. Although this filter does not use any second-order partial derivatives, the estimates are quite good for all the models investigated and are comparable to the TMV estimates. Of particular interest are the estimates based on the pure model, since, of the model-filter configurations considered, the combination of pure model and DPLS filter is the easiest to implement.

Finally, it was found that nonlinear measurements provided estimates comparable in quality to the estimates based on linear measurement. Results have been presented of a limited study of the application of linear and nonlinear filters to the problem of estimating the time delay of a simple hereditary system. In the case of the pure model, an iterated Kalman filter avoided the divergence problem. With the Padé approximate models, the Kalman filter convergence appears to improve as the order of the approximation is increased. Both of the investigated nonlinear filters provided good estimates regardless of the model chosen. In particular, the direct application of the simplest nonlinear filter to the original pure form problem resulted in estimates comparable to the estimates based on a more complex model and filter.

References

[1] Ray, W. H. and Soliman, M.A., "The Time Optimal Control of Processes Containing Pure Time Delays," *Proceedings of the 11th Joint Automatic Control Conference of the American Automatic Control Council,* Atlanta, Ga., 1970.

[2] Schiess, J. R., Wells, W. R., and Roland, V. R., "Estimation of Nonlinear Pilot Model Parameters Including Time Delays," *Proceedings of the Second Symposium on Nonlinear Estimation Theory and Its Applications,* San Diego, Calif., Sept. 1971.

[3] Koivo, A. J. and Stoller, R. L., "On Least Squares Estimation in Nonlinear Dynamical Systems With Time Delay," *Proceedings of the 9th Joint Automatic Control Conference of the American Automatic Control Council,* Univ. of Michigan, Ann Arbor, Mich., June 1968.

[4] Kwakernaak, H., "Optimal Filtering in Linear Systems With Time Delays," *IEEE Transactions on Automatic Control,* Vol. AC-12, No. 2, April 1967.

[5] Mehra, R. K., and Tyler, J. S., "Modeling the Human Operator Under Stress Conditions Using System Identification," *Proceedings of the 13th Joint Automatic Control Conference of the American Automatic Control Council,* Stanford Univ., Stanford, Calif., Aug. 1972.

[6] Schwartz, L., and Stear, E. B., "A Computational Comparison of Several Nonlinear Filters," *IEEE Transactions on Automatic Control,* Vol. AC-14, No. 2, April 1968.

Nitrogen Temperature Determination in Arc Tunnel Air Flows

S. S. LAZDINIS* AND R. F. CARPENTER†
Air Force Flight Dynamics Laboratory, Wright-Patterson Air Force Base, Ohio

Introduction

An instrument known as the Rotational Temperature Device (RTD), which employs the electron-beam diagnostic technique originated by Muntz,[1] has been constructed at the Air Force Flight Dynamics Lab. It has been used to obtain radial profiles of nitrogen rotational temperatures in an arc tunnel air flow and its results have been compared with standard spectrographic electron-beam measurements. Since the nitrogen rotational temperature and the static translational temperature are in equilibrium for the flows analyzed in this study, the RTD serves as an on-line monitor of the static temperature. A similar instrument was constructed by Muntz and Abel[2] to measure rotational temperatures in short duration, shock tunnel flows. However, the degree of accuracy between their measurements and those obtained using the usual electron-beam technique has never been experimentally determined.

Presented as Paper 72-1022 at the AIAA 7th Aerodynamics Testing Conference, Palo Alto, Calif., September 13–15, 1972; submitted October 2, 1972; revision received May 29, 1973.

Index categories: Atomic, Molecular, and Plasma Properties; Nozzle and Channel Flow.

* Aerospace Engineer, Flight Mechanics Division. Member AIAA.

† Physicist, Flight Mechanics Division.

Rotational Temperature Device

Details concerning the electron-beam method and the optical properties of the instrument have been given in Refs. 3 and 4. Briefly, the device functions in the following manner. Radiation induced by the electron-beam is imaged on its entrance aperture by an external lens, which is placed approximately 7 ft from the beam. The light is then collimated within the instrument and is divided by a partially reflecting beam splitter in the ratio 30/70. Each beam passes through one of two narrow band pass filters which have a nominal centerpass wavelength of 3910 Å and a half-width of approximately 12 Å (the location of the centerpass of each channel is set at the desired wavelength by tipping the filters). The filtered radiation is then chopped by a dual frequency chopper and focused onto a single photomultiplier.

The signals of each channel are separated by two lock-in amplifiers, locked to the two chopping frequencies. A reference signal for the lock-ins is obtained from the same chopping wheel by the use of infrared light emitting diodes and matched photodiodes. The amplifier output is fed into a ratio computer and two strip chart recorders which record the filtered intensity seen by each of the channels and the relative intensity ratio as determined by the ratio computer. The latter device also drives a nonlinear scale voltmeter calibrated to permit observation of the instantaneous value of the static temperature. The time constant of each channel is set at 1 sec to provide a reasonable signal-to-noise ratio. A schematic of the RTD is given in Fig. 1.

The advantage of this system over the instrument developed by Muntz and Abel[2] is the use of a single photomultiplier tube to record the output of both channels. This feature eliminates problems associated with relative phototube drift and the need for prerun and postrun phototube calibrations. The instrument can thus be used to monitor static temperatures on-line and in real time.

To deduce a rotational temperature from the RTD measurements, the behavior of the filtered intensity ratio as a function

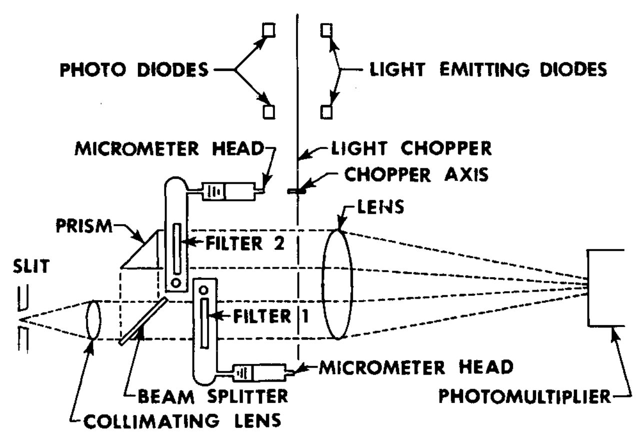

Fig. 1 Schematic of rotational temperature device.